Chemical Engineering Journal 101 (2004) 123–131

Chemical Engineering Journal

www.elsevier.com/locate/cej

Experiments and modelling of an integrated preferential oxidation–heat exchanger microdevice

E.R. Delsman [a], M.H.J.M. de Croon [a], G.J. Kramer [a], P.D. Cobden [b], Ch. Hofmann [c], V. Cominos [c], J.C. Schouten [a,*]

[a] *Laboratory of Chemical Reactor Engineering, Eindhoven University of Technology, P.O. Box 513, 5600 MB Eindhoven, The Netherlands*
[b] *Energy Research Center of the Netherlands, Petten, The Netherlands*
[c] *Institut für Mikrotechnik Mainz, Mainz, Germany*

Abstract

Microreactor technology creates opportunities for the development of miniature chemical devices, in which several unit operations are integrated. We describe in this paper the design, experimental, and modelling work concerning a microdevice for the preferential oxidation of carbon monoxide in hydrogen-rich reformate gas. The microdevice consists of two heat exchangers and one reactor, all integrated in a single stack of microstructured plates. Experiments show that the initial carbon monoxide conversion is high. However, the catalyst deactivates rapidly. It takes over one hour to reach the required reactor temperature during startup, which is too long for application in a portable fuel processor. The measured temperature gradients in the heat exchangers are twice as small as predicted by a one-dimensional heat exchange model of the microchannels. A two-dimensional model shows that large differences in temperature exist between channels close to the inlet and channels further from the inlet, causing the one-dimensional model to fail. This paper shows that for an accurate description of heat transfer in a micro heat exchanger, the complete (two-dimensional) plate geometry needs to be considered.

Keywords: Microreactor; Integration; Preferential oxidation; Heat exchange; Modelling

1. Introduction

In recent years microfabrication technologies are being introduced in the fields of chemistry and chemical process engineering to realize microchannel devices, e.g. mixers, heat exchangers, and reactors, with capabilities considerably exceeding those of conventional macroscopic systems [1,2]. Microreactors have reaction channels with diameters of the order of 100–500 μm, a channel length of about 1–10 cm, and have an inherently large surface area-to-volume ratio. These properties offer clear advantages such as high mass and heat transfer rates, which is beneficial for attaining high selectivities and conversions and enables optimum control of temperature and residence time [3–5]. Microreactors also have a low hold-up, resulting in excellent controllability, small safety risks, and low environmental impact [6,7]. This makes these micro reaction devices specifically suitable for highly exothermic reactions, short contact time reactions, and for the on-demand and safe production of toxic and hazardous chemicals.

Microreactors also show large promise in the development of miniature chemical devices, where several unit operations are integrated with microstructured sensors and actuators to form a micro chemical plant [8–10]. Integrating a variety of components in a small device asks for new design approaches and solutions for constructional issues, like for example connecting different kinds of materials, the integration of microstructured sensors and actuators, and the thermal separation of adjacent units, that operate at different temperatures. These miniaturized chemical devices offer opportunities for small scale fuel processing and portable power generation, for example, to replace battery packs in laptops or mobile phones [11,12]. Microreactors can be used to convert liquid or gaseous fuels, like methanol or methane, to hydrogen, which can be fed to a fuel cell to produce electricity. The challenge is to develop microchemical systems in which all reaction and heat transport steps are optimally integrated, in combination with appropriate sensors and actuators for process monitoring and control.

Within the European Union funded project MiRTH-e [13], a miniaturized fuel processing system is developed to generate hydrogen in situ from a methanol–water mixture, to fuel a 100 W_e fuel cell. The fuel processing system consists

* Corresponding author. Tel.: +31-40-247-2850; fax: +31-40-244-6653.
E-mail address: j.c.schouten@tue.nl (J.C. Schouten).

1385-8947/$ – see front matter © 2004 Elsevier B.V. All rights reserved.
doi:10.1016/j.cej.2004.01.005

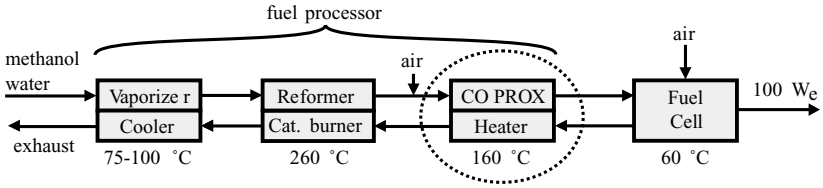

Fig. 1. A fuel processor—fuel cell system, consisting of three integrated microdevices and a miniature fuel cell, all working at specific temperatures. The encircled unit is the integrated preferential oxidation–heat exchanger device studied in this paper.

of a steam reformer, which converts methanol and water to a hydrogen-rich gas, a preferential CO oxidation unit to remove the 0.5% of carbon monoxide present, and a catalytic burner to supply energy for the methanol–water vaporization and the endothermic methanol reforming. Based on an energy analysis of the system, the fuel processor is subdivided into three integrated microdevices operating at different temperatures, i.e. a vaporizer–cooler, a reformer–burner, and a preferential oxidation–heat exchanger unit, see Fig. 1. The targeted volume for the portable fuel processor is 500 cm^3.

In this paper, we describe the design, experimental, and modelling work of the preferential oxidation–heat exchanger (ProxHeatex) microdevice, which is designed and manufactured in cooperation with the Institut für Mikrotechnik Mainz (IMM) and the Energy Research Center of the Netherlands (ECN). Main purpose of the device is to remove the carbon monoxide present in the reformate gas, since carbon monoxide is a severe poison for the fuel cell catalyst. To decrease the concentration of carbon monoxide to below 10 ppm, it is oxidized using a small quantity of air added to the reformate gas. To promote the oxidation of carbon monoxide and suppress the oxidation of hydrogen, a selective catalyst has to be used, like Pt/Al_2O_3 [14–16] or Au/Fe_2O_3 [17]. In this study, a $Pt–Co/\alpha\text{-}Al_2O_3$ catalyst is used, developed at ECN. The addition of cobalt to the catalyst was found to increase both activity and selectivity of the $Pt/\alpha\text{-}Al_2O_3$ preferential oxidation catalyst. Since most of the fuel processor volume will be needed by the reformer unit, the aspired volume of the ProxHeatex unit amounts to 100 cm^3 including insulation material.

The ProxHeatex device also needs to recover 80% of the heat that is released by the oxidation reaction (11 W) and by cooling down the hot reformate gas from 250 to 60 °C, the operating temperature of the fuel cell (13 W), to increase the energy efficiency of the fuel processor. The ProxHeatex device is designed to consist of three counter-current heat exchangers in series, see Fig. 2, to provide an isothermal reaction zone and reach an efficient heat recovery. In the high temperature heat exchanger, the hot reformate gas is cooled down to the reaction temperature of 150 °C. The gas then enters the middle heat exchanger, which contains the preferential oxidation catalyst and serves as a cooled reactor. In the low temperature heat exchanger, the CO-free reformate gas is cooled down further to 60 °C. The recovered heat is used to preheat the combined fuel cell anode and cathode exhaust gas, which still contains about 5% of

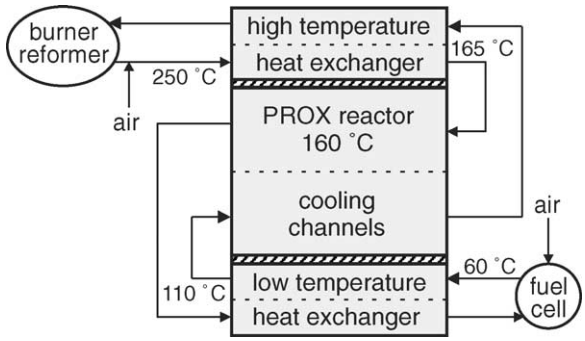

Fig. 2. Schematic drawing of the integrated preferential oxidation–heat exchanger microdevice. The device consists of two heat exchangers and a cooled reactor. The temperatures of the reformate and coolant gas streams are also indicated.

hydrogen, to about 200 °C, before it is sent to the catalytic burner.

The purpose of this work is also to study the heat transfer behavior of micro heat exchangers and the effect of integrating several heat exchangers in a single device. Micro heat exchangers differ from larger-scale heat exchangers, as axial conduction of heat through the solid material becomes more important in a microdevice [18,19], while gas–solid heat transfer becomes less important. Therefore, in this paper, we do not solely address practical issues like reactor performance, startup time, and heat recovery efficiency, but we also present a modelling study of the heat transfer in the micro heat exchangers. In the first part of the paper, we provide a detailed description of the construction of the ProxHeatex microdevice as well as the experimental setup that is used to study the performance of the device. Two heat transfer models are developed to describe heat transfer in a microdevice, which are described in the second part of this paper. The experiments show that the one-dimensional heat exchange model is not able to predict the measured temperature gradients. The poor performance of the one-dimensional model is explained using a two-dimensional model, which also provides a clear insight into the heat transfer characteristics of the micro heat exchangers and may serve as a tool for further microreactor development.

2. ProxHeatex design

The heat exchangers of the ProxHeatex device are constructed from 500 μm thick microstructured plates, as shown

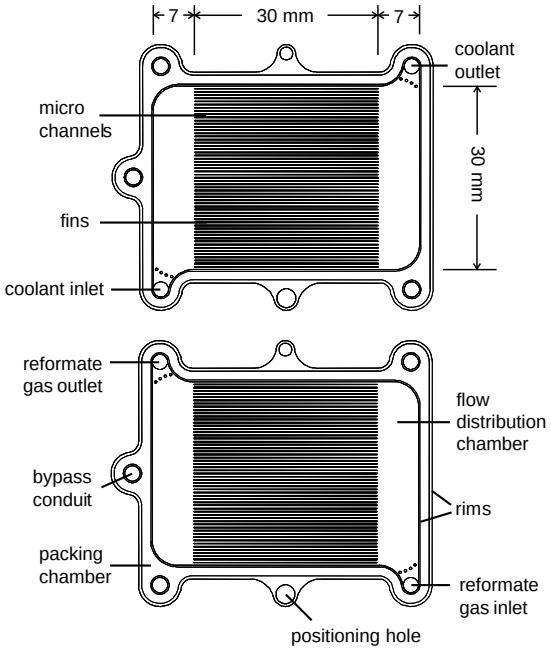

Fig. 3. Microstructured heat exchanger plates; stacking of the two plate types creates a heat exchanger; plate dimensions ($w \times l$) are 35 mm × 48 mm, with 58 microchannels of ($w \times h \times l$) 0.4 mm × 0.3 mm × 30 mm; the diameter of the inlets and outlets is 2 mm and the width of the packing chambers is also 2 mm.

in Fig. 3. The microstructured plates contain an outer groove that serves as a packing chamber, inlet and outlet flow distribution chambers, and a central part containing the actual channels. These microstructures were made in the stainless steel sheets by means of wet etching. Holes were drilled in the plates to provide inflow and outflow conduits for the two gas streams, to facilitate positioning of the plates on top of each other, and to provide a reactor bypass conduit. The bypass conduit is, however, not used in this study. The heat exchangers are formed by alternate stacking of mirror images of the plates. The exchangers are covered with an unstructured steel sheet to close the channels of the top plate. To be able to integrate the individual parts in a single stack, the plate geometry of all heat exchangers is identical, differing only in the channel cross-section and the number of channels. Graphite is used as sealing material for the reactor part and Klingersil®, a compressed fiber jointing material with a low thermal conductivity, is used in the low and high temperature heat exchangers.

The assembled device, schematically shown in Fig. 4, contains 41 microstructured plates. The low and high temperature heat exchangers both contain six plates: two reformate side plates and four coolant plates. The reactor part consists of nineteen catalyst coated reaction plates and ten coolant plates. Three of the four walls of the reaction channels were coated at the Energy Research Center of the Netherlands with a 15 μm thick layer of a Pt–Co/α-Al_2O_3 catalyst. The total amount of catalyst in the reactor is 0.98 g. The two flanges are fixed with eight screws to compress the gaskets

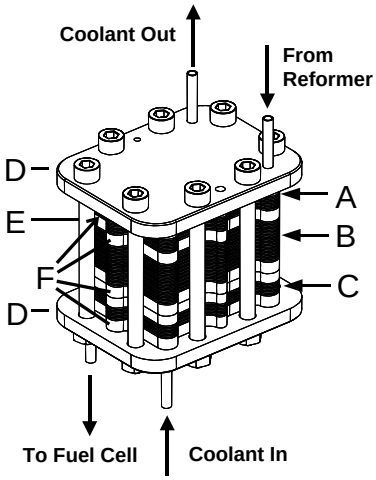

Fig. 4. Assembled microreactor, developed in cooperation with the Institut für Mikrotechnik Mainz and the Energy Research Center of the Netherlands. It consists of a high temperature heat exchanger (A), a cooled reactor (B), and a low temperature heat exchanger (C); outer dimensions are 66 mm × 53 mm × 50 mm; (D) flanges, (E) fixing screw; (F) position of the four insulation plates.

and make the device leak-tight. Specifications of the individual units are listed in Table 1. The complete device measures 66 mm × 53 mm × 50 mm and weighs 980 g. To reduce external heat losses from the device, the complete device is insulated by a 3 cm thick layer of HT/Armaflex® insulating material.

Insulating plates are inserted between the heat exchangers and the reactor, and between the heat exchangers and the flanges, to thermally separate the various device parts. Three different sets of insulation plates were manufactured. The first insulation plate type is a 4 mm thick stainless steel plate. A 2 mm deep air chamber was milled from the top of the plate over 90% of the plate's surface area, to increase its thermal resistance. The second insulation plate is a 2 mm thick plate cut from the same Klingersil® material as used for the seals in the heat exchangers. The third type of insulation plate consists of a stack of three 2 mm thick Klingersil® plates, of which two plates have a hole cut out over 90% of the plate's surface area. Two holes were drilled in each of the insulating plates to connect the inlets and outlets of the reactor and the heat exchangers. The thermal resistance (layer thickness divided by material conductiv-

Table 1
Specifications of the integrated preferential oxidation device

Parameter	HT exchanger[a]		Prox reactor		LT exchanger	
	Ref	Cool	Ref	Cool	Ref	Cool
Number of plates	2	4	19	10	2	4
Number of channels	58	58	83	75	58	58
Channel width (μm)	400	400	250	250	400	400
Channel height (μm)	300	300	187	125	300	300

[a] HT: high temperature, LT: low temperature, Ref: reformate side, Cool: coolant side.

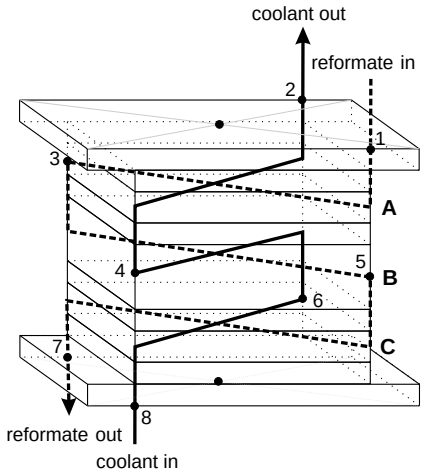

Fig. 5. Schematic representation of the flow paths of the reformate and coolant gas through the microdevice. Temperature measurement points are indicated by black dots and are numbered for further reference. A, B, and C designate the high temperature heat exchanger, the reactor, and the low temperature heat exchanger, respectively.

ity and cross-sectional area) of the three insulation layers is 0.87, 3.0, and 63 K/W, respectively.

The flow path of the reformate and coolant gas through the device is shown in Fig. 5. In this figure, also the locations of the thermocouples are indicated, which measure the inlet and outlet temperatures of the device at a position just outside the flanges, four internal temperatures at the outlets of the reactor and heat exchangers, and the temperatures of the top and bottom flanges. The four internal thermocouples measure the metal temperature instead of the gas temperature, as it was not possible to avoid contact of the thermocouples with the walls of the conduit in which they were inserted. However, at the outlet side of the reactor and heat exchangers, the difference between gas and metal temperature is expected to be small.

The reformate gas consisted of 0.5% CO, 1.6% O_2, 56% H_2, 18% CO_2, and balance helium. The reformate gas was analyzed for oxygen and CO at the inlet and outlet of the ProxHeatex device to determine conversion and selectivity. The analysis was done with a gas chromatograph equipped with a Poraplot U and a Molesieve 5 Å column and a micro-TCD detector using helium as carrier gas. As the reformate gas was projected to enter the ProxHeatex device at a temperature of 250 °C, the gas was first preheated to 300 °C just before entering the proxHeatex device. A cable heater was used to reduce heat losses in the tube between the preheater and the ProxHeatex device. In the experiments pure nitrogen was used as coolant gas. To preheat the coolant gas to 60 °C, the coolant feed tube was heated over a distance of 1.5 m with a cable heater. No CO was fed when the temperature profile in the device was studied, since the presence of CO causes deactivation of the catalyst and the preferential oxidation reaction itself was of minor importance in this case. CO oxidation was replaced by hydrogen oxidation to mimic the heat production in the prox reactor. Although hydrogen reacts faster than CO, the total amount of heat production was considered more important than the heat production rate.

3. Heat transfer modelling

A one-dimensional heat transfer model was developed to describe the temperature profile in the microdevice. The model calculates the temperature profiles of the reformate gas (r), the coolant gas (c), and the metal of the heat exchanger plates (m). For conventional heat exchangers the walls are usually not modelled separately, as axial conduction through the walls of the tubes can usually be neglected. However, for micro heat exchangers axial conduction is an important factor determining the heat exchanger efficiency [18,19]. As the distance between the reformate and coolant channels is very small and the conductivity of stainless steel is two orders of magnitude larger than that of the gases, the radial temperature profile in the material between the channels was neglected. By also assuming an even flow distribution over the microchannels, heat exchange in the channel region was described by a one-dimensional model.

Plug flow was assumed for both gases and axial dispersion was neglected. Due to the fast radial heat transport, axial dispersion introduced by the laminar flow profile could also be neglected. The temperature profile of the gases is then determined by convective heat transport and heat exchange with the metal walls. When the length coordinate is made dimensionless with the length of the heat exchanger, the equations for the reformate and coolant gas become

$$(\dot{m}c_p)_\mathrm{r}\frac{\mathrm{d}T_\mathrm{r}}{\mathrm{d}\hat{x}} = -\alpha_\mathrm{r}A_\mathrm{r}(T_\mathrm{r} - T_\mathrm{m}) \tag{1}$$

$$(\dot{m}c_p)_\mathrm{c}\frac{\mathrm{d}T_\mathrm{c}}{\mathrm{d}\hat{x}} = -\alpha_\mathrm{c}A_\mathrm{c}(T_\mathrm{m} - T_\mathrm{c}) \tag{2}$$

with $(\dot{m}c_p)_i$ the heat transport capacity (mass flow rate × heat capacity) of fluid i (W/K), α_i the gas–solid heat transfer coefficients (W/m^2 K), and A_i the respective heat exchange surface areas (m^2). To calculate the heat transfer coefficients, entrance effects were neglected and a constant Nusselt number of 3.1 was assumed for the rectangular microchannels [20].

The model for the metal plates takes into account axial heat conduction through the plates, heat exchange with the two gases, with adjacent device parts and with the environment, and, for the reactor part, heat production due to reaction, to give

$$\begin{aligned}-\frac{\lambda_\mathrm{m}A_\mathrm{m}}{L}\frac{\mathrm{d}^2T_\mathrm{m}}{\mathrm{d}\hat{x}^2} = {} & \alpha_\mathrm{r}A_\mathrm{r}(T_\mathrm{r} - T_\mathrm{m}) - \alpha_\mathrm{c}A_\mathrm{c}(T_\mathrm{m} - T_\mathrm{c}) \\ & - \alpha_\mathrm{ex}A_\mathrm{ex}(T_\mathrm{m} - T_\mathrm{ex}) \\ & - \alpha_\mathrm{in}A_\mathrm{in}(T_\mathrm{m} - T_\mathrm{in}) + \dot{Q}_\mathrm{p}\end{aligned} \tag{3}$$

with λ_m the conductivity of the reactor material (W/m K), A_m the cross-sectional area of the reactor material perpendicular to the x-axis (m^2), and L the heat exchanger length (m). The heat transfer coefficient for heat exchange between adjacent device parts (α_{in}) is calculated from the conductivity, thickness and cross-sectional area of the insulating layer and of the device parts themselves. The external losses are calculated with a heat transfer coefficient (α_{ex}) of 3.5 W/m^2 K, based on the external surface of the device without insulation, which is derived from the experimentally determined cooling curve of the device, recorded after closing the gas feeds. Heat production due to reaction ($\dot{Q}_p$) is modelled as

$$\dot{Q}_p(\hat{x}) = \dot{Q}_{tot} k e^{-k\hat{x}}, \quad (4)$$

with the decay factor k arbitrarily set at 10 to simulate a fast reaction.

The top and bottom flanges were also included in the model. Due to their thickness, they were modelled as being isothermal. For the flanges heat exchange with the adjacent heat exchanger and with the environment is included in the model as well as heat exchange between the two flanges through the tightening screws. Furthermore, an additional heat input from the heater cables to the flanges is included. The additional heat input was calculated, based on the steady state temperature of the flanges without flow to the device, to be 4 W at the reformate inlet, and 0.5 W at the coolant inlet. Since all parts of the device exchange heat with each other, the temperatures in the heat exchangers, the reactor, and the two flanges were calculated simultaneously in three linked one-dimensional models, using the Femlab® finite element solver [21].

Next to the one-dimensional model of the complete device also a two-dimensional model has been developed describing a single micro heat exchanger. The two-dimensional model describes the temperature fields in a plane, parallel to the microstructured plates. In the direction perpendicular to the plates, the temperatures are assumed to be constant. The model geometry consists of the channel area and the two flow distribution areas, as shown in Fig. 6. Like in the 1D model, the 2D model takes into account convective heat transport by the flowing gases, heat transfer between gases and reactor material, heat conduction through the reactor material, and heat transfer to adjacent device parts and to the environment. The velocity field in the flow distribution areas is not calculated, but is approximated by a linearly decreasing y-velocity from the inlet to the opposite wall, and a linearly increasing x-velocity from the side wall to the channel region. In the channel region the reformate gas flows straight from left to right and the coolant gas straight from right to left. In this way, the continuity equation is satisfied in the complete domain. Gas–solid heat transport is modelled with a constant Nusselt number of 3.1 for the channel region and 7.5 [20] for the flow distribution regions. For the heat conductivity of the solid material volume averaged values are used, which are different for flow distribution and channel

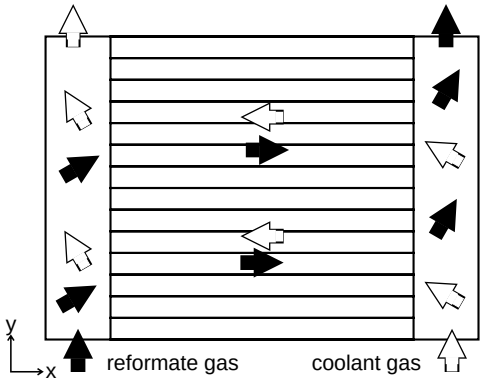

Fig. 6. Model geometry of the two-dimensional micro heat exchanger model with the two flow distribution regions and the central channel region. The flow paths of the reformate and coolant gas are indicated by the full and open arrows, respectively.

region and, within the channel region, are different for the x- and y-direction due to the presence of the fins. Here only the equations for the left flow distribution region are presented:

$$(\dot{m}c_p)_r \hat{x} \frac{\partial T_r}{\partial \hat{x}} + (\dot{m}c_p)_r (1-\hat{y}) \frac{\partial T_r}{\partial \hat{y}} = -\alpha_r A_r (T_r - T_m), \quad (5)$$

$$-(\dot{m}c_p)_c \hat{x} \frac{\partial T_c}{\partial \hat{x}} + (\dot{m}c_p)_c \hat{y} \frac{\partial T_c}{\partial \hat{y}} = \alpha_c A_c (T_m - T_c), \quad (6)$$

and

$$-\frac{\lambda_m A_{mx}}{L_x} \frac{\partial^2 T_m}{\partial \hat{x}^2} - \frac{\lambda_m A_{my}}{L_y} \frac{\partial^2 T_m}{\partial \hat{y}^2} = \alpha_r A_r (T_r - T_m) - \alpha_c A_c (T_m - T_c) - \alpha_{ex} A_{ex} (T_m - T_{ex}) - \alpha_{in} A_{in} (T_m - T_{in}), \quad (7)$$

with $\hat{x}$ and $\hat{y}$ the dimensionless coordinates, and the other terms similar as for the one-dimensional model. The equations for the right flow distribution region are similar, except that the factors $\hat{x}$, $(1-\hat{y})$, and $\hat{y}$ in Eqs. (5) and (6) are replaced by $(1-\hat{x})$, $\hat{y}$, and $(1-\hat{y})$, respectively. In the channel region the gases flow straight from right to left and vice versa, which means that Eqs. (5) and (6) simplify to Eqs. (1) and (2). Eq. (7) is similar in all regions, except that the constants change to reflect the differences is gas–solid heat transfer and metal cross-section.

4. Results and discussion

4.1. Preferential oxidation activity

The performance of the ProxHeatex device is evaluated in terms of preferential oxidation activity and selectivity. The reformate gas flow rate is reduced from 2.9 to 0.8 standard liter per minute (SLM), as the amount of catalyst present in the reactor is less than is needed for full conversion of the projected amount of carbon monoxide. This also

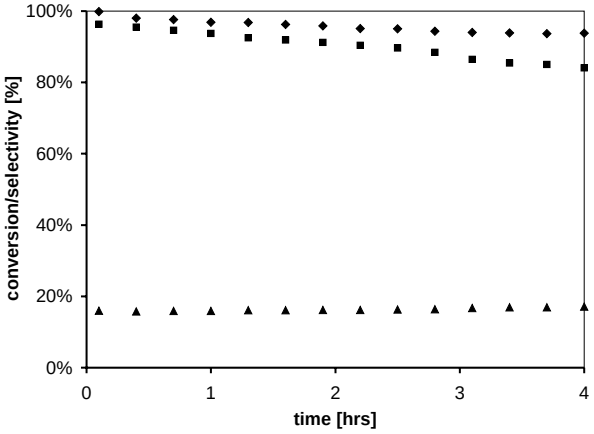

Fig. 7. Carbon monoxide (diamonds) and oxygen (squares) conversion, and the selectivity of oxygen towards carbon dioxide (triangles), as function of time. Reformate flow rate was 0.8 SLM and reactor temperature was 160 °C.

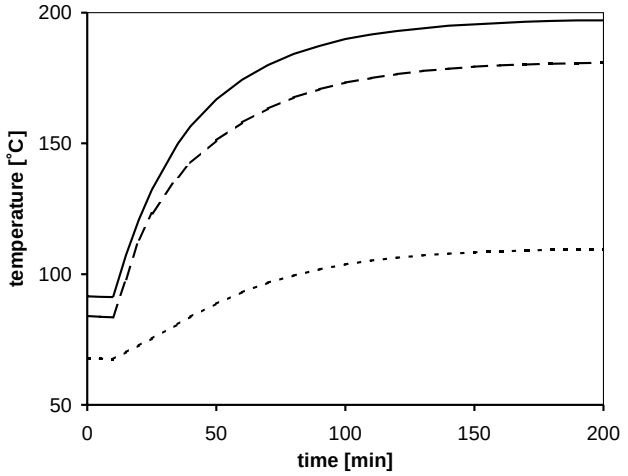

Fig. 8. Temperature of the coolant outlet (full line), the reactor (dashed line), and the reformate outlet (dotted line) during startup of the device. Reformate and coolant flow rates were 2.9 and 6.3 SLM, respectively. Heat production was 11 W.

reduces the amount of heat produced in the reactor. Since the device does not contain an external heater to control its temperature, this would lead to a decreased reactor temperature. The oxygen inlet concentration is increased to 1.6% to increase the heat production in the reactor via additional hydrogen burning and increase the reactor temperature to 160 °C. Fig. 7 shows the conversion and selectivity of the preferential oxidation reaction as a function of time. The figure shows that the initial carbon monoxide conversion is high and the CO outlet concentration is reduced to 7 ppm. However, the catalyst deactivates rapidly and the CO outlet concentration rises to 300 ppm over a period of 4 h. While the catalyst deactivates, the selectivity remains constant at the initial value of 17%. Although catalyst deactivation is a problem for large scale operations, it is even more so for the portable ProxHeatex device, since in situ regeneration of the catalyst or frequent replacement of the complete reactor are both unattractive options to be used for a portable fuel processor device. Therefore, it is important to improve the stability of the preferential oxidation catalyst, as well as to achieve a higher catalyst loading in the reactor.

4.2. Start-up behavior

Another important factor for application of the ProxHeatex device in a portable fuel processor is its startup behavior. Fig. 8 shows the reactor and flange temperatures as a function of time during startup of the device. The figure shows that the startup time of the device is large and that it takes over one hour to reach a reactor temperature of 160 °C. In the experiment the projected operating conditions are used, which are a reformate flow rate of 2.9 SLM, translating to a heat transport capacity (mass flow × heat capacity) of 0.07 W/K, and a coolant flow rate of 6.3 SLM (0.14 W/K). In the reactor 11 W of heat is generated by hydrogen burning. However, these numbers are small compared to the heat capacity of the device itself, which is about 460 J/K, resulting in the long startup time.

Although fluids can be heated or cooled very rapidly in microreactors, the transient behavior of the device itself depends on the ratio of the heat capacity of all solid material (the microstructured plates, packings, flanges, screws, and insulation) and the heat transport capacity of the fluid flows. This ratio is not favorable for a gas-phase microreactor, due to the high solid fraction of a microreactor and the low heat capacity of gases. For application of microdevices in fuel processors or other dynamic processes, care has to be taken to minimize the solid fraction of a microdevice and to use light-weight materials with low heat capacity for the construction of the device. The studied ProxHeatex microdevice also contains two heavy stainless steel flanges for compression of the seals between the microplates. The flanges and screws add up to about 70% of the total mass of the device. Using a construction without the need for these flanges, for instance by welding the plates together, will improve the device's transient behavior.

4.3. Heat transfer efficiency

Also the heat transfer efficiency of the micro heat exchangers is studied. In three experiments, the influence of the type of insulation plates between the device parts is studied on the temperature profile in the heat exchanger and reactor parts and thus on the heat transfer performance of the device. In the experiments the device is re-assembled three times, each time using a different set of insulation plates. In each case, the steady state temperature profile was measured at the same operating conditions as described for the startup experiment. Fig. 9 shows the temperature profile in the ProxHeatex device with the three different sets of

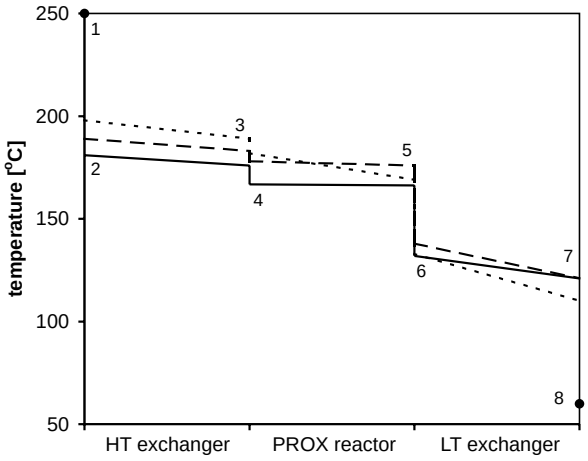

Fig. 9. Measured temperature profiles in the ProxHeatex microdevice assembled with different sets of insulation plates: steel plates with air chambers (solid line), single Klingersil® sheets (dashed line), and multiple Klingersil® sheets with air chambers (dotted line). The inlet temperature of the reformate gas was 250 °C and of the coolant gas 60 °C. The numbers indicate the temperature measurement points specified in Fig. 5.

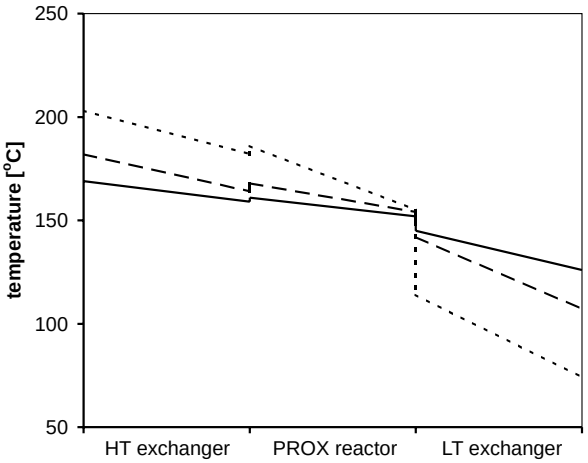

Fig. 10. Calculated temperature profiles in the ProxHeatex microdevice assembled with three different insulation layers: steel plates with air chambers (solid line), single Klingersil® sheets (dashed line), and multiple Klingersil® sheets with air chambers (dotted line). The inlet temperatures are 250 and 60 °C for reformate and coolant gas, respectively.

insulation plates. The figure shows that the heat exchange performance of the device increases when the thermal resistance between the units is increased, as both the temperature difference between the device parts and the axial temperature gradient within the device parts increase. The fraction of heat, of the total amount of heat available in the reformate gas and released by the oxidation reaction, that is recovered in the device by heating-up the coolant gas, increased from 68% with the steel insulation plates to 78% with the multiple Klingersil® sheets. It is difficult to assess the performance of the individual heat exchangers, since conductive heat transfer between adjacent units, which we cannot measure, plays an important role in the integrated microdevice.

We also predicted the temperature profiles found in the experiment with the one-dimensional heat transfer model described in the section on heat transfer modelling. In Fig. 10 the calculated temperature profiles are presented for the three cases with different insulation plates. The predicted average temperatures of the individual device parts are within 15 °C of the experimental values, except for the multiple Klingersil® sheets insulation case, where the deviation is 30 °C for the low temperature heat exchanger temperature. This is a good result taken into account that the model does not contain any fit parameters. However, the temperature gradients in the device parts are not well predicted. The predicted temperature gradients are about twice as large as is found in the experiments, which makes the model unsuited to predict the heat exchanger efficiencies. The model also predicts a clear influence of the type of insulation plates used, on the temperature difference between the device parts, while the experiments show almost no influence.

4.4. Two-dimensional model results

A two-dimensional heat transfer model was made to explain the deviations between the one-dimensional model and the experiments. The simulation results for the high temperature heat exchanger are depicted in Fig. 11. In this figure, the contour lines show the temperature difference between the hot reformate gas and the metal of the heat exchanger and the grays indicate the metal temperature. Furthermore, at the inlets and outlets the temperature of the gases and the

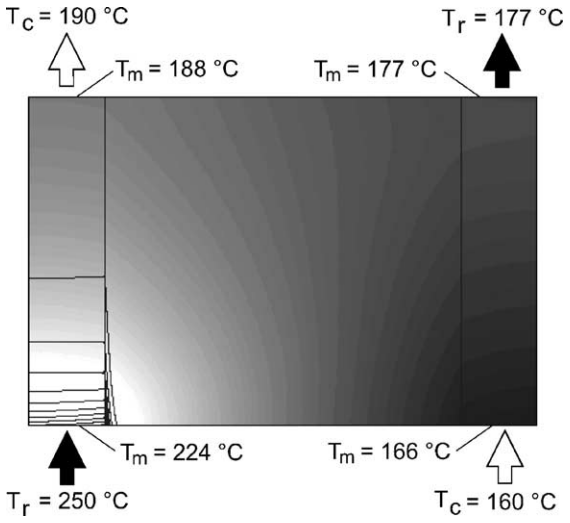

Fig. 11. Results of the two-dimensional calculations of the high temperature heat exchanger. The grays show the temperature distribution in the metal plates. The metal (T_m), reformate gas (T_r), and coolant gas (T_c) temperatures at the inlets and outlets are also indicated. The contour lines show the temperature difference between the hot reformate gas and the metal plates (steps of 2.6 °C).

metal is indicated. The contour lines show that the temperature equilibration between gas and metal is very fast and takes place almost completely within the first part of the flow distribution region. Although the flow distribution chambers do not contain microchannels, the height of the distribution chambers is very small, in this case 300 μm, which means that heat transfer is already very effective in these regions of the plate. The effective heat exchange in the flow distribution chambers leads to considerable differences in temperature between the first and the last channels, which is the reason for the over-prediction of the temperature gradients by the one-dimensional channel model. It is interesting to note that the temperature of the coolant gas at the outlet is 2 °C higher than the metal temperature, due to the part of the coolant gas that flows over the hotter bottom part of the plate.

The grays in Fig. 11 show the metal temperature of the exchanger. As the gas temperatures equilibrate very fast with the metal temperature, the gas temperatures are close to the metal temperature except for a small region near the inlets. The figure shows that the temperature difference between left and right side of the plate, or hot and cold side of the exchanger, is about 58 °C at the bottom side of the plate, but decreases towards the exits at the top side of the figure to 11 °C. Since the plates are almost square and a significant part of the heat transfer takes place in the flow distribution chambers, the behavior of the heat exchanger more closely resembles that of a mixed co-current and cross-flow behavior than a true counter-current behavior, leading to a low heat exchange efficiency. For the design of a micro plate heat exchanger, it is thus important to take the complete plate geometry into consideration. To increase the counter-current character of the heat exchangers and to improve the heat exchange efficiency of the ProxHeatex microdevice, the length of the exchanger plates should be increased and the width of the plates, or the distance between inlet and outlet, should be decreased.

5. Conclusions

A microdevice was designed and manufactured for the preferential oxidation of carbon monoxide in a hydrogen-rich reformate gas, consisting of two heat exchangers and a cooled reactor, all integrated in a single stack of microstructured plates. The device was able to reduce the carbon monoxide concentration from 0.5% to 7 ppm, but only during the first half hour of operation, after which the conversion dropped due to catalyst deactivation. Due to the large mass of the device, the startup time of the device was about one hour, which is too long for application in a portable fuel processor. The temperature profiles in the heat exchangers were measured and a one-dimensional heat exchange model was developed to predict these profiles. A considerable deviation exists between experiments and the one-dimensional model. A two-dimensional simulation of one of the heat exchangers showed that large differences exist between channels close to the inlet and channels further from the inlet, causing the one-dimensional model to fail. This example shows that it is important to consider the complete plate geometry when designing a micro plate heat exchanger.

Based on the outcome of this study, the design of the ProxHeatex device was improved and a second prototype will be built. The new device will contain longer channels and a reduced plate width to improve the heat exchanger efficiency. To reduce the mass of the unit, the microstructured plates will be welded together instead of using gaskets to provide leak-tightness. Furthermore, a better catalyst will be applied in the reactor and also a higher catalyst loading will be used.

Acknowledgements

The authors gratefully acknowledge funding from the European Commission for the Micro Reactor Technology for Hydrogen and Electricity (MiRTH-e) project within the Fifth Framework Programme under contract number ENK6-2000-00110.

References

[1] W. Ehrfeld, V. Hessel, H. Löwe, Microreactors: New Technology for Modern Chemistry, Wiley-VCH, Weinheim, Germany, 2000.
[2] K.F. Jensen, Chem. Eng. Sci. 56 (2001) 293–303.
[3] A. Kursawe, E. Dietzsch, S. Kah, D. Hönicke, M. Fichtner, K. Schubert, G. Wießmeier, in: W. Ehrfeld (Ed.), Proceedings of the 3rd International Conference on Microreaction Technology, Springer, Berlin, Germany, 2000, pp. 213–223.
[4] H. Kestenbaum, A. Lange de Oliveira, W. Schmidt, F. Schüth, W. Ehrfeld, K. Gebauer, H. Löwe, Th. Richter, D. Lebiedz, I. Untiedt, H. Züchner, Ind. Eng. Chem. Res. 41 (2002) 710–719.
[5] E.V. Rebrov, S.A. Duinkerke, M.H.J.M. de Croon, J.C. Schouten, Chem. Eng. J. 93 (2003) 201–216.
[6] M. Janicke, A. Holzwarth, M. Fichtner, K. Schubert, F. Schüth, Stud. Surf. Sci. Catal. 130 (2000) 437–442.
[7] G. Veser, Chem. Eng. Sci. 56 (2001) 1265–1273.
[8] A. Lohf, W. Ehrfeld, V. Hessel, H. Löwe, in: J. Baselt, W. Ehrfeld, K.-P. Jaeckel, I. Rinard, R. Wegeng (Eds.), Proceedings of the 4th International Conference on Microreaction Technology, AIChE, New York, USA, 2000, pp. 441–451.
[9] A.Y. Tonkovich, J.L. Zilka, M.R. Powell, C.J. Call, in: W. Ehrfeld, I.H. Rinard, R.S. Wegeng (Eds.), Proceedings of the 2nd International Conference on Microreaction Technology, AIChE, New York, USA, 1998, pp. 45–53.
[10] J.W. Ashmead, J.K. Nyquist, J.A. Perrotto, C.T. Blaisdell, M.H. Johnson, J.F. Ryley Jr., US Patent 5,690,763 (1997).
[11] R.S. Wegeng, L.R. Pederson, W.E. TeGrotenhuis, G.A. Whyatt, Fuel Cells Bulletin 3 (2001) 8–13.
[12] J.D. Holladay, E.O. Jones, M. Phelps, J. Hu, J. Power Sources 108 (2002) 21–27.
[13] E.R. Delsman, E.V. Rebrov, M.H.J.M. de Croon, J.C. Schouten, G.J. Kramer, V. Cominos, T. Richter, T.T. Veenstra, A. van den Berg, P.D. Cobden, F.A. de Bruijn, C. Ferret, U. d'Ortona, L. Falk, in: M. Matlosz, W. Ehrfeld, J.P. Baselt (Eds.), Proceedings of the 5th International Conference on Microreaction Technology, Springer Verlag, Berlin, Germany, 2001, pp. 268–274.
[14] S.H. Oh, R.M. Sinkevitch, J. Catal. 142 (1993) 254–262.
[15] M.J. Kahlich, H.A. Gasteiger, R.J. Behm, J. Catal. 171 (1997) 93–105.

[16] C.D. Dudfield, R. Chen, P.L. Adcock, Int. J. Hydrogen Energy 26 (2001) 763–775.
[17] M.J. Kahlich, H.A. Gasteiger, R.J. Behm, J. Catal. 182 (1999) 430–440.
[18] W. Bier, W. Keller, G. Linder, D. Seidel, K. Schubert, H. Martin, Chem. Eng. Proc. 32 (1993) 33–43.
[19] T. Stief, O.-U. Langer, K. Schubert, Chem. Ing. Technol. 70 (1998) 1539–1544.
[20] R.K. Shah, A.L. London, Laminar flow forced convection in ducts, in: T.F. Irvine, J.P. Hartnett (Eds.), Advances in Heat Transfer, Supplement 1, Academic Press, New York, 1978.
[21] Femlab®, version 2.3b, Comsol AB, Stockholm, Sweden, 2003.